



Metabolic profiles of human brain parenchyma and glioma for rapid tissue diagnosis by targeted desorption electrospray ionization mass spectrometry

Rong Chen¹ · Hannah Marie Brown¹ · R. Graham Cooks¹

Received: 8 June 2021 / Revised: 23 July 2021 / Accepted: 30 July 2021 / Published online: 9 August 2021
© Springer-Verlag GmbH Germany, part of Springer Nature 2021

Abstract

Desorption electrospray ionization mass spectrometry (DESI-MS) is well suited for intraoperative tissue analysis since it requires little sample preparation and offers rapid and sensitive molecular diagnostics. Currently, intraoperative assessment of the tumor cell percentage of glioma biopsies can be made by measuring a single metabolite, N-acetylaspartate (NAA). The inclusion of additional biomarkers will likely improve the accuracy when distinguishing brain parenchyma from glioma by DESI-MS. To explore this possibility, mass spectra were recorded for extracts from 32 unmodified human brain samples with known pathology. Statistical analysis of data obtained from full-scan and multiple reaction monitoring (MRM) profiles identified discriminatory metabolites, namely gamma-aminobutyric acid (GABA), creatine, glutamic acid, carnitine, and hexane-1,2,3,4,5,6-hexol (abbreviated as hexol), as well as the established biomarker NAA. Brain parenchyma was readily differentiated from glioma based on these metabolites as measured both in full-scan mass spectra and by the intensities of their characteristic MRM transitions. New DESI-MS methods (5 min acquisition using full scans and MS/MS), developed to measure ion abundance ratios among these metabolites, were tested using smears of 29 brain samples. Ion abundance ratios based on signals for GABA, creatine, carnitine, and hexol all had sensitivities > 90%, specificities > 80%, and accuracies > 85%. Prospectively, the implementation of diagnostic ion abundance ratios should strengthen the discriminatory power of individual biomarkers and enhance method robustness against signal fluctuations, resulting in an improved DESI-MS method of glioma diagnosis.

Keywords Metabolomics · Biomarker · Glioma · Ambient ionization · Multiple reaction monitoring · Tandem mass spectrometry

Introduction

Glioma is the most common intracranial tumor and it accounts for more than 50% of all primary brain tumors [1]. Gross total tumor resection is considered to be the most effective treatment for glioma patients, despite not often being achieved clinically [2]. Glioma cells are diffusely infiltrative and often result in residual tumor at surgical margins that may lead to disease progression and tumor reoccurrence. Currently, neurosurgeries are guided by magnetic resonance imaging (MRI), which is not sufficiently sensitive to gauge the infiltration of glioma, especially in regions with low tumor cell density [3]. Moreover, spatial registration between a patient's brain and

the preoperative MR images may be compromised as brain shift is common during craniotomies [4]. Consequently, intraoperative tissue diagnosis increasingly relies on molecular features assessed from tumor biopsies [5] to locate the tumor boundary with a higher sensitivity and to provide additional pathological information, like tumor grade and genetic mutation [6]. Ultimately, this should allow surgeons to maximize tumor resection and personalize adjunctive therapies.

Several molecular diagnostic techniques have been applied clinically, including magnetic resonance spectroscopy (MRS) and fluorescence imaging [7]. MRS is conducted preoperatively to assess tumor type and aggressiveness, but it is not well suited for intrasurgical tissue analysis. 5-Aminolevulinic acid-induced fluorescence guidance has been used as a surgical guide to improve glioma resection by identifying tumor location [8] although it has limited value in accurate tissue diagnosis [9]. Techniques that rapidly and quantitatively interrogate molecular features of tissue are currently being

✉ R. Graham Cooks
cooks@purdue.edu

¹ Department of Chemistry, Purdue University, 560 Oval Drive, West Lafayette, IN 47907-2084, USA

developed. One such technique, Raman spectroscopy, is capable of providing label-free and molecular-specific information of tissue [10]. Raman spectroscopy can be conducted either *in vivo*, with a handheld Raman probe placed directly on the tissue surface for data acquisition [3], or *ex vivo* to analyze brain biopsies with little sample preparation, automatic data acquisition and analysis, and near-immediate feedback [11]. Additionally, ambient ionization mass spectrometry (MS) has been identified as a potential method for intraoperative tissue diagnosis [5, 12], given its capability of sensitive and rapid metabolite characterization. MS-based techniques use various approaches of rapid and simple tissue sampling. For example, the MasSpec Pen relies on water extraction to sample analytes from tissue non-destructively [13, 14], picosecond infrared laser mass spectrometry (PIRL-MS) utilizes laser ablation to vaporize molecules from the irradiated tissue [15, 16], SpiderMass uses water as an endogenous matrix to assist in laser desorption of analytes in tissue [17], and rapid evaporative ionization mass spectrometry (REIMS) analyzes electrosurgical vapors [18]. The molecular information offered by MS is typically characterized using relative ion signals of analytes, without attempting to convert ion abundances into their concentrations in tissue.

Desorption electrospray ionization mass spectrometry (DESI-MS), the technique utilized in this work, uses charged solvent droplets to rapidly extract analytes, including metabolites, from the tissue surface [19]. The metabolic profile recorded by MS allows differentiation between cancerous tissue and normal tissue [20, 21] and identification of tumor grade and subtype [22]. While still an experimental modality, DESI-MS has been used to distinguish between cancerous and normal tissue in a variety of human cancers including pancreatic [23], breast [24], brain [25–27], ovarian [21, 28], and gastric cancers [29]. To facilitate its potential intraoperative application, morphologically friendly spray solvents have been used so that the same specimen can be subjected to histopathologic analysis following MS measurement [30]. Intraoperatively, fresh tissue smears are used for DESI-MS analysis, which simplifies sample preparation and facilitates the formation of a homogeneous layer of tissue so that rapid profiling can capture its overall chemical features [31].

Metabolic (and lipidic) fingerprints, which are unique to different tissue types, are the fundamental basis of all the diagnostic methods mentioned above. The altered cellular metabolism of tumors [32–34] has been explored both by *in vivo* methods, including metabolic imaging (e.g., MRS) and isotope-labeled metabolite tracing (using ^{13}C -labeled analogs) [35], as well as by *ex vivo* methods including MS and nuclear magnetic resonance spectroscopy [36]. Several metabolites involved in various biosynthetic pathways have been reported to differentiate glioma and other cancer cells from normal cells. For example, D-2-hydroxyglutarate (D-2HG) is a well-established biomarker for isocitrate dehydrogenase (IDH)

mutations [35, 37], since the mutated IDH exclusively converts α -ketoglutarate to D-2HG. Increased lactic acid production has been reported for several cancer types, including glioma [38, 39], kidney [40], prostate [41], and ovarian cancer [14], because cancerous cells generally require anaerobic glycolysis to sustain energy production in hypoxia [42]. NAA is synthesized in neuronal mitochondria and hydrolyzed to supply acetate for acetyl coenzyme A (CoA) synthesis [43, 44]. Its decreased level in glioma [25] may be explained by a lower neuron density [42] or accelerated utilization of CoA for increased gene transcription and energy metabolism in glioma cells [35, 44]. Glutamate is the most abundant neurotransmitter, and its extracellular concentration is maintained at low levels by excitatory amino acid transporters (EAAT) to prevent excitotoxicity [45]. However, glioma cells lose the ability to absorb glutamate since EAAT is under-expressed, causing a local downregulation of glutamate [45]. Creatine is involved in the creatine/creatine kinase (CK)/phosphocreatine system for adenosine triphosphate (ATP) regeneration [46, 47]. Several studies have reported lower creatine concentrations in malignant glioma [47–49] and oral [50] and bladder cancer [51], possibly due to adapted ATP production and increased phosphocreatine consumption for tumor bioenergetics [47, 52]. Gamma-aminobutyric acid (GABA) signaling has been reported to lead to membrane depolarization and to result in cell growth attenuation [53]. Fast-growing glioma tumors downregulate the GABA signaling pathway, causing the depletion of GABA [53]. Carnitine facilitates the transport of fatty acids into mitochondria for energy metabolism [54]; therefore, its increased level offers an additional energy source to promote tumor progression [55]. Mannitol, widely used to control brain edema in patients by creating an osmotic gradient across the blood-brain barrier (BBB) [56], is upregulated in glioma due to the tumor's defective BBB. Our DESI-MS method for intraoperative assessment of glioma [26, 27, 37] presently uses the measurement of a single oncometabolite, NAA, for estimating tumor cell percentage (TCP) and another, 2HG, for assessing IDH mutation status. The inclusion of additional glioma biomarkers is worth investigation as it has the potential to improve differentiation of brain parenchyma from glioma and so increase diagnostic accuracy.

Here, we report a study which used rapid, comprehensive metabolic profiling to discover diagnostic metabolites capable of distinguishing normal human brain and glioma tissue. First, mass spectra of extracts from 32 human brain samples were recorded using nanoESI (nESI) for biomarker discovery. To mine more metabolic information, multiple reaction monitoring (MRM) profiling, which offers a higher sensitivity and specificity [57], was applied. The diagnostic metabolites uncovered—GABA, creatine, glutamic acid, carnitine, and hexane-1,2,3,4,5,6-hexol (abbreviated as hexol)—were integrated into a new DESI-MS method and used to analyze 29 brain smears, mimicking the intraoperative workflow. In parallel,

ion abundance ratios of these diagnostic metabolites were tested for their discriminatory power using known pathologic information. Their prediction sensitivity (> 90%), specificity (> 80%), and accuracy (> 85%) show promise for improving the current DESI-MS method for intraoperative glioma diagnosis.

Materials and methods

Specimens

A set of 32 frozen and unmodified human brain tissue was purchased by Purdue University from the Biorepository of Methodist Research Institute. Extracts were prepared from these specimens by keeping the aqueous phase of the Bligh and Dyer extraction [58]. Separately, 29 specimens from this tissue collection were smeared on glass microscope slides for DESI-MS analysis using the new multi-metabolite method (illustrated in Supplementary information Fig. S1).

Pathology

Pathologic evaluations of specimens in the tissue collection were made in our previous work and are summarized in Supplementary information Table S1 [25]. Cryo-sectioned tissue was mounted onto glass slides and hematoxylin and eosin (H&E) stained following the standard protocol. The stained slides were blindly evaluated by an expert pathologist to provide pathological information including tissue type (i.e., brain or subtypes of glioma), tumor grade, and estimated TCP.

MS analysis

MS analysis of brain extracts was performed using a triple quadrupole mass spectrometer (TSQ Quantum Access MAX, Thermo Fisher Scientific) by nESI. The orifice of glass tips was optimized at 8 μm and the spray voltage was optimized at 1.4 kV for a stable spray. In full-scan MS profiling, the mass range was set at m/z 50–350 and three replicas were acquired for one sample in both ion modes. In the discovery phase of MRM profiling, precursor and neutral loss scans from the scan library (summarized in Supplementary information Table S2) were applied to the pooled healthy brain and glioma extracts to discover informative transitions with abundant and stable signals. In the subsequent screening phase, individual brain extracts were interrogated for these selected transitions in both ion polarities. To identify diagnostic molecules, their exact masses were measured using a high-resolution mass spectrometer (Q Exactive Orbitrap, Thermo Fisher Scientific) and product ion scans were acquired using the TSQ. DESI-MS analysis of brain smears was performed with a linear ion-trap mass spectrometer (Finnigan LTQ, Thermo Fisher Scientific). Methanol was used as the spray

solvent with a flow rate of 3 $\mu\text{L}/\text{min}$, nitrogen was the nebulizing gas at a pressure of 150 psi, and the spray voltage was 5 kV. The position of the DESI sprayer was optimized at a sprayer-to-surface distance of 2 mm, a sprayer-to-inlet distance of 4 mm, and a spray impact angle of 54°. To support rapid tissue analysis, brain smears were rastered under the DESI spray to capture average data from various locations on the tissue surface. The developed multiple-metabolite DESI method for positive-ion mode was composed of five segments: full scan over the range of m/z 50–350, MS/MS of m/z 104, MS/MS of m/z 132, MS/MS of m/z 162, and MS/MS of m/z 170. Each segment took 1 min, making the overall analysis time of a smear approximately 5 min. The negative-ion DESI method shared a similar configuration, covering five segments: a scan over the range of m/z 50–350, MS/MS of m/z 146, MS/MS of m/z 174, MS/MS of m/z 217, and MS/MS of m/z 271. Note that all data discussed in this study was recorded explicitly for this purpose; no data was re-purposed.

Statistical analysis

In both profiling methods, the raw MS data was normalized, filtered, and averaged before principal component analysis (PCA) to show the separation between the two tissue types. The optimal separating hyperplane in the score plot was determined by the method of soft-margin support vector machine. The support vectors were identified using the MATLAB function “fitcsvm” to maximize the soft margin between the separating hyperplane and data points. The most discriminatory spectral features were discovered by t tests based on their p values. For ion abundance ratios in DESI-MS, discriminatory cutoffs were optimized for maximum area-under-curve (AUC) in the receiver operating characteristic (ROC) curves. Sensitivity, specificity, and accuracy at the optimal cutoff were calculated to assess diagnostic performances of these ion abundance ratios.

Results and discussion

Spectral features discovered by full-scan MS profiling

As a straightforward and efficient method of discovering biomarkers, full-scan mass spectra were acquired using nESI for all brain extracts in the two groups established by pathology as healthy or glioma. After normalization and filtering (see Supplementary information section entitled “Experimental Details”), PCA was applied to the mass spectral data. In the PCA score plot based on positive-mode spectra (Fig. 1b), the points representing 14 glioma samples separate well from those representing the 18 healthy samples. The observation of two misclassified samples may be because the assumed glioma tissue is likely to contain significant healthy tissue and therefore have mixed morphology. Spectral features

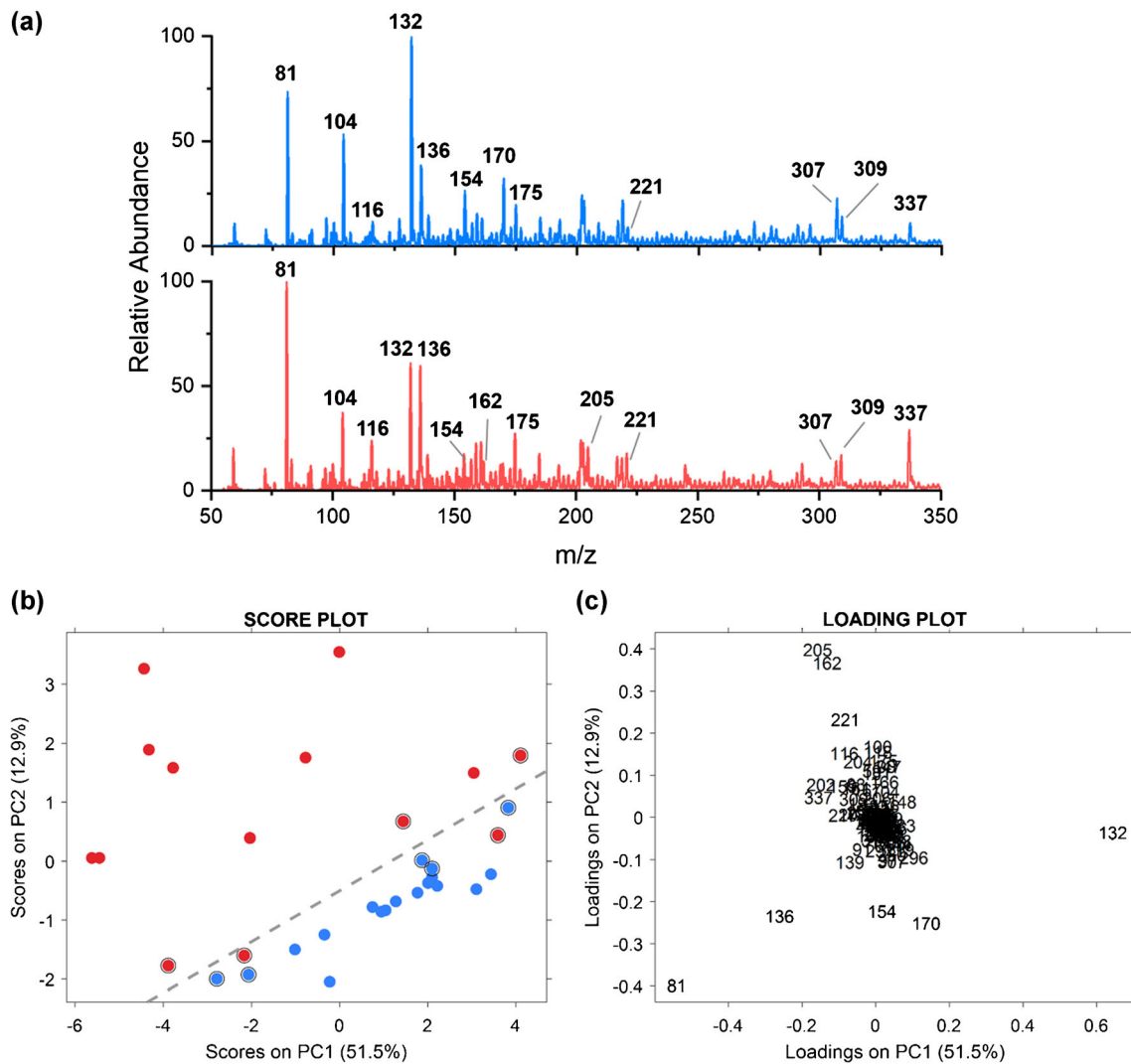


Fig. 1 Full-scan profiling of brain extracts in the positive-ion mode. **a** Representative mass spectra of healthy brain (blue) and glioma extracts (red) recorded by nESI. **b** PCA score plot of the 18 healthy and 14 glioma brain extracts using abundant positive-mode spectral features. The

separating hyperplane (gray dotted line) was optimized by the soft-margin support vector machine using the circled data as support vectors. **c** PCA loading plot showing spectral features which contribute most to the separation

contributing to the separation are shown in the loading plot (Fig. 1c), where metabolites indicated by m/z 132, 154, and 170 are characteristic of healthy brain tissue. As expected, signal intensities of these metabolites are lower in glioma samples, as shown in the representative full-scan spectra (Fig. 1a) and in their box plots (Supplementary information Fig. S2a). Conversely, metabolites indicated by m/z 162, 205, and 211 are characteristic of glioma tissue and exhibit higher signal intensities in glioma samples (Fig. 1a and Supplementary information Fig. S2b). Based on their measured exact masses and fragmentation patterns in tandem MS (MS/MS) spectra, the spectral features most representative of healthy tissue were identified as protonated creatine (m/z 132), its sodium adduct (m/z 154), and its potassium adduct (m/z 170), while the most characteristic features for glioma tissue are protonated carnitine (m/z 162), the potassium adduct

of hexol (m/z 221), and an unknown compound (m/z 205). A complete list of the 20 most discriminatory features in the positive-ion mode, as well as their identities, is summarized in Supplementary information Table S3.

After applying PCA to mass spectral profiles acquired in the negative-ion mode, similar separation between the two groups was observed in the score plot (Fig. 2b). The loading plot (Fig. 2c) revealed that healthy brain samples are primarily differentiated by m/z 146 and 174, while glioma samples are differentiated by m/z 147, 181, 217, 219, and 271. Signal variations of these features can be visualized in the representative mass spectra (Fig. 2a) and their box plots (Supplementary information Fig. S3). After structural identification by exact mass measurement and MS/MS, these discriminatory features were identified as glutamate (m/z 146), 2HG (m/z 147), NAA (m/z 174), deprotonated hexol ($[M - H]^-$, m/z 181), its chloride adducts

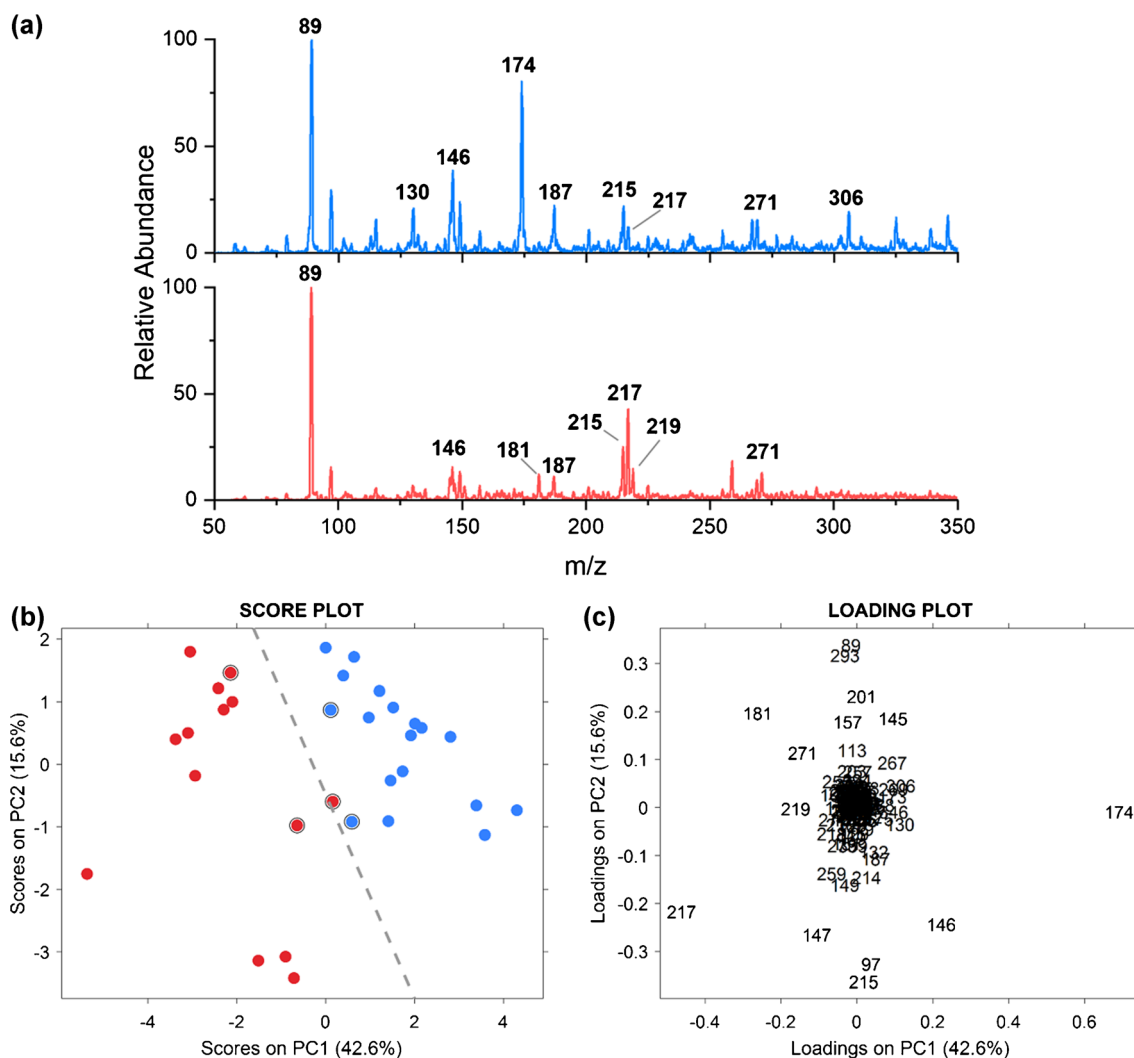


Fig. 2 Full-scan profiling of brain extracts in the negative-ion mode. **a** Representative mass spectra of healthy brain (blue) and glioma extracts (red) recorded by nESI. **b** PCA score plot of the 18 healthy and 14 glioma brain extracts using abundant negative-mode spectral features. The

separating hyperplane (gray dotted line) was optimized by the soft-margin support vector machine using circled data as support vectors. **c** PCA loading plot showing significant spectral features which contribute to the separation

($[M\cdot^{35}Cl]^-$, m/z 217; $[M\cdot^{37}Cl]^-$, m/z 219), and the lactate adduct ($[M\cdot C_3H_5O_3]^-$, m/z 271). Considering that all stereoisomers in the family of hexols (e.g., mannitol and sorbitol) share the same exact masses and fragmentation pathways, a more specific identification was not possible in this case. The observed down-regulation of NAA and upregulation of 2HG in glioma samples are consistent with previous reports [25, 37] and confirm the feasibility of the current DESI-MS method for glioma tissue diagnosis [26, 27, 37]. A complete list of the 20 most discriminatory features in the negative-ion mode is provided in Supplementary information Table S4.

Fragmentation features discovered by MRM profiling

Brain extract is a complex biosample with high concentrations of salts, whose interference can attenuate MS signals. The increased specificity of tandem MS was exploited by

applying MRM profiling to identify additional diagnostic metabolites not seen in the full-scan spectra. MRM profiling is a two-stage exploratory technique to perform rapid metabolomics and lipidomics based on chemical functionalities of small molecules [57]. First, in the discovery stage, precursor and neutral loss (NL) scans targeting common functional groups were applied to representative samples to discover informative precursor-product transitions (viz. MRMs). The library of precursor and NL scans used in this study can be found in Supplementary information Table S2. In total, 953 transitions (573 in the positive-ion mode and 380 in the negative-ion mode) passed the thresholds set for signal intensity and stability. Second, in the screening phase, abundances of all informative transitions were recorded for each of the 32 tissue extracts and statistical analysis was performed to identify the most discriminatory transitions.

After applying PCA to data for the informative transitions in both polarities, the resulting score plots (Fig. 3a, b) displayed good separations between the two groups. A few misclassified samples were also observed; they were determined by pathology to have low to medium tumor density, which explains the similarities of their profiles to healthy tissue. Transitions with the highest discriminatory power (lowest p values) were identified by t tests and summarized in Supplementary information Tables S5 and S6. In the positive-ion mode, the 20 most diagnostic transitions include

those associated with GABA, creatine (protonated and potassium adduct), glutamic acid, homocarnosine, and inosine. The box plots shown in Fig. 3c exhibit the good discriminatory power of GABA, glutamic acid, and creatine. The discovery of diagnostic transitions not only will benefit targeted analysis using benchtop mass spectrometers, but should also promote point-of-care analysis using portable instruments where low-resolution and noisy full-scan spectra are common [59]. Comparing results of the two profiling methods, a few metabolites such as creatine and inosine were identified by both.

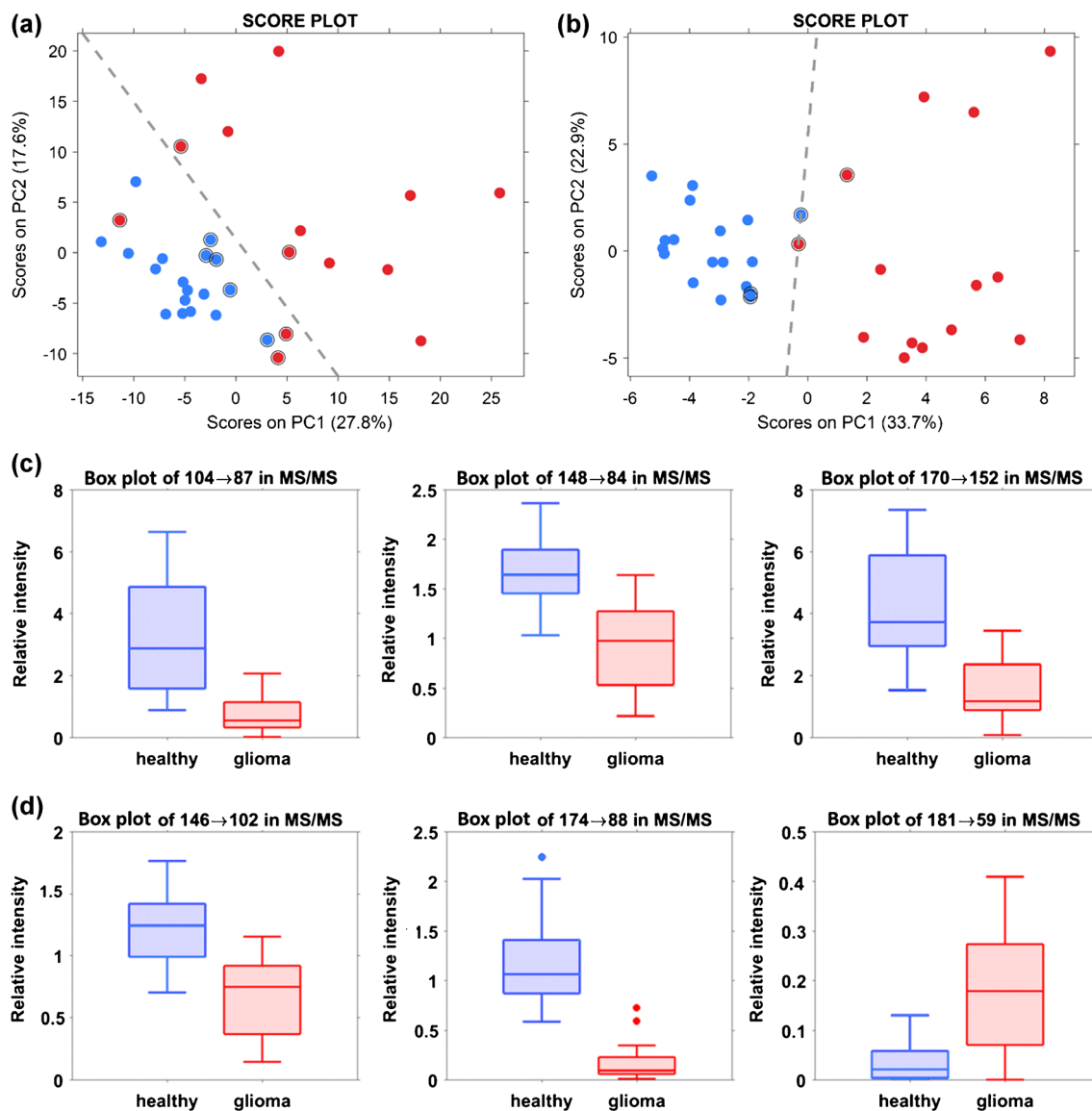


Fig. 3 **a** PCA score plot using informative transitions in the positive-ion mode where blue points represent healthy extracts and red points represent glioma extracts. The separating hyperplane (gray dotted line) was optimized by the soft-margin support vector machine using the circled data as support vectors. **b** PCA score plot using informative transitions in the negative-ion mode. **c** Box plots of transitions associated with diagnostic metabolites in the positive-ion mode, including GABA (104 → 87), glutamic acid (148 → 84), and creatine (potassium adduct: 170 →

152). The y-axis of box plots refers to transition intensities normalized to that of the internal standard transition (glutamic acid- d_3 : 151 → 133). The box represents the interquartile range with a median line, and the maximal length of whiskers is 1.5 times the interquartile range. **d** Box plots of transitions associated with diagnostic metabolites in the negative-ion mode, including glutamate (146 → 102), NAA (174 → 88), and deprotonated hexol (181 → 59). The internal standard transition in negative polarity was glutamate- d_3 : 149 → 105

MRM profiling expanded the number of diagnostic metabolites to include GABA, whose full-scan spectral intensity was not reliable given the presence of an isobaric ion namely choline. In the negative-ion mode, the 20 most diagnostic transitions included those associated with glutamate, NAA, hexol, inosine, and N-acetylaspartylglutamate, which are consistent with the full-scan profiling results. Box plots of the characteristic transitions of glutamate, NAA, and deprotonated hexol demonstrated good separation between the glioma and healthy groups (Fig. 3d).

The integration of data from full-scan profiling and MRM profiling represents a comprehensive screening of potential glioma biomarkers. Full-scan profiling is easier to conduct and has a relatively impartial coverage of molecules that ionize well. Conversely, MRM profiling relies on the scan library to target common functional groups, potentially biasing against molecules with unusual structures or those that ionize to form adducts. That said, MRM profiling can facilitate more sensitive and specific measurements, benefiting from its operation in the MS/MS mode. This also makes MRM profiling less vulnerable to matrix effects and better able to distinguish isobaric ions. Taken together, full-scan and MRM profiling unveiled several diagnostic metabolites, including GABA, creatine, glutamic acid, carnitine, hexol, inosine, and N-acetylaspartylglutamate, in addition to the established 2HG and NAA. Given that the extraction occurring during DESI-MS is nearly instantaneous and presumably less efficient than Bligh and Dyer extraction, only the most abundant features observed in brain extracts could be interrogated further by DESI-MS. These are GABA, creatine (protonated and potassium adduct), and carnitine in the positive-ion mode, and glutamate, NAA, and hexol (deprotonated and chloride/lactate adducts) in the negative-ion mode.

Translation to DESI-MS analysis

The discriminatory power of the metabolites selected in the previous section was further tested using smeared brain tissue to mimic a multi-metabolite-based extension of intraoperative DESI-MS analysis [26, 27, 37]. Methanol was selected as the spray solvent of DESI due to its morphologically friendly nature and the ability to provide rich metabolic information with minimal background noise. More detailed information on the DESI instrumentation and optimized parameters is included in the “Experimental Details” section of the Supplementary information. Supplementary information Fig. S1 is a schematic illustration of rapid DESI-MS analysis, showing the smearing of brain tissue (ca. 30 s operation time) and rastering of smears under the DESI spray (5 min data-acquisition time). Unlike DESI-MS imaging, this experiment records the average chemical features of the entire sample rather than being used to provide spatially resolved information.

DESI-MS is a semi-quantitative technique unless internal standards are used [60]. In order to deploy the diagnostic power of identified markers in DESI-MS without the use of an internal standard, we used ion abundance ratios, rather than absolute peak intensities, to enhance the method’s robustness against signal fluctuations or background noise. Additionally, by using abundance ratios, the discriminating power can be strengthened when the numerator and denominator of the ratio show opposite variations. For example, in the positive-ion mode (Figs. 1 and 3), carnitine is upregulated in glioma samples while creatine is downregulated, making the ratio between neighboring peaks of m/z 162 (protonated carnitine) and m/z 170 (potassium adduct of creatine) highly diagnostic of the tissue disease state. This was experimentally confirmed by the representative DESI-MS spectra recorded in the positive mode (Fig. 4a) and by the box plot of this ratio (Fig. 4c). Further, the peak at m/z 175, identified as protonated arginine, displayed weak if any discrimination based on its intensity in the full-scan mass spectra (Supplementary information Fig. S4a) or its MRM transitions (Supplementary information Fig. S4b). Therefore, arginine can be treated as an endogenous internal standard for creatine, causing the signal ratio m/z 170:175 to decrease in glioma samples. Protonated GABA has an isobaric ion, choline, whose presence makes the full-scan intensity data unreliable. However, the isobars give different fragment ions in the MS/MS mode. The transition associated with choline shows a relatively constant level (Supplementary information Fig. S4c), making it an endogenous standard for GABA. In other words, when fragmenting the peak of m/z 104 (Fig. 4b), choline (MS/MS: 104 → 60) and protonated GABA (MS/MS: 104 → 87) each produce their respective fragments simultaneously making the fragment ratio m/z 87:60 diagnostic. Figure 4c–e show box plots of these three ion abundance ratios with good separation between the two tissue types. The marked cutoff in the plots was optimized for a maximum area under the curve (AUC) in the receiver operating characteristic (ROC) curve. Based on the optimal cutoff, values for sensitivity, specificity, and accuracy were calculated. The three ion abundance ratios all display sensitivities > 90%, specificities > 80%, and accuracies > 85%. Wilcoxon rank-sum tests were also applied for these ratios; all ratios display p values < 0.001. Based on these statistical results (summarized in Supplementary information Table S7), the three ion abundance ratios are sufficiently powerful to discriminate between the healthy and glioma samples. Note that two are determined from the single-stage MS while the third is an MS/MS measurement.

In the negative-ion mode, the ratio between downregulated NAA and upregulated hexol in glioma tissue was investigated. Representative full-scan spectra (Fig. 5a) show that hexol is detected by DESI-MS primarily as its chloride adducts ($[\text{M}^{35}\text{Cl}]^-$, m/z 217; $[\text{M}^{37}\text{Cl}]^-$, m/z 219) and its lactate adduct ($[\text{M}\cdot\text{C}_3\text{H}_5\text{O}_3]^-$, m/z 271), rather than as the deprotonated

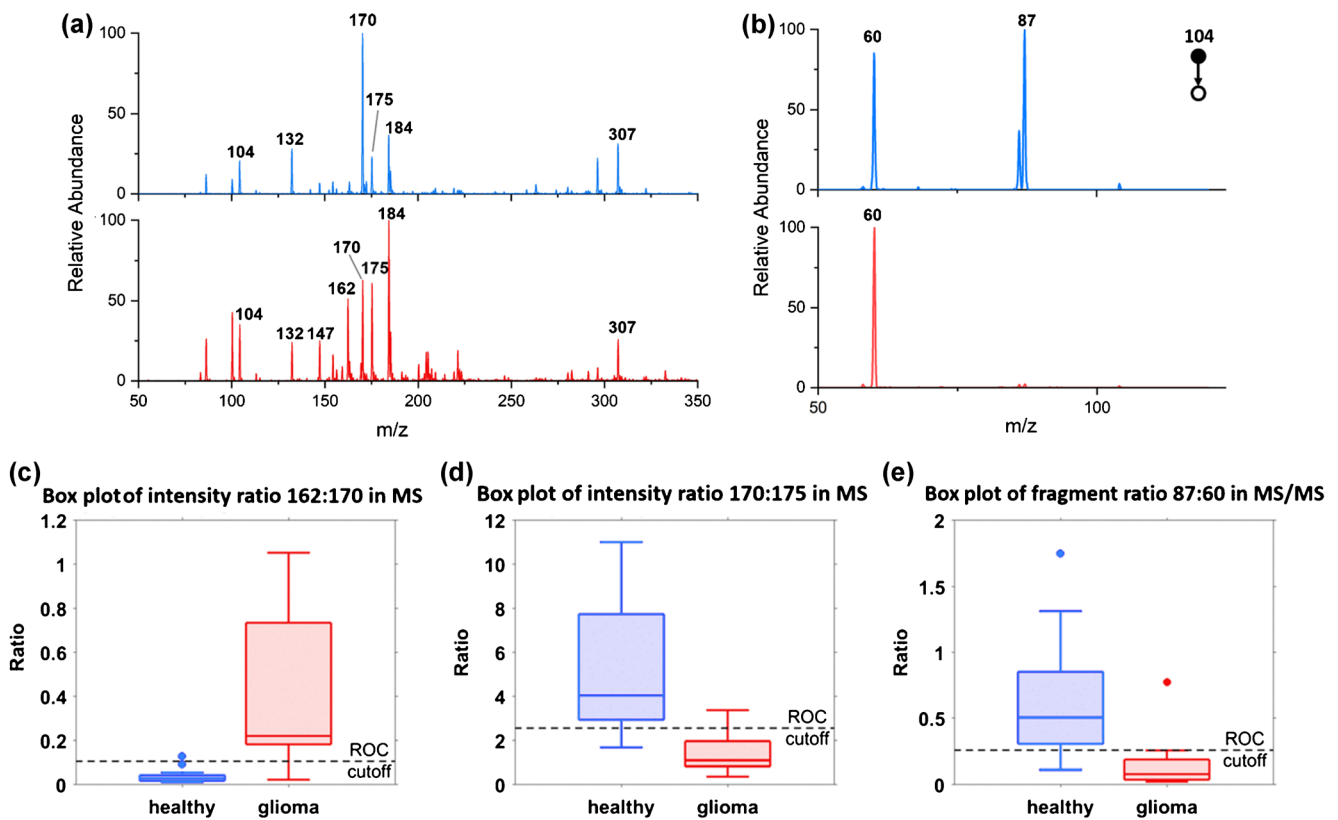


Fig. 4 **a** Positive-mode DESI-MS mass spectra for a representative healthy (blue) and glioma (red) tissue smear. **b** Product ion scans of m/z 104 for a representative healthy and glioma tissue smear. The choline-associated transition ($104 \rightarrow 60$) is used as the endogenous standard for the GABA-associated transition ($104 \rightarrow 87$). **c** Box plot using MS abundance ratio m/z 162:170 as a discriminator: m/z 162 indicates protonated carnitine and m/z 170 indicates creatine K^+ . The ROC cutoff was optimized at 0.11, with a sensitivity, specificity, and accuracy of 92, 94, and 93%, respectively. Wilcoxon rank-sum test indicated a statistically significant variation between the two groups (p value < 0.001). **d** Box plot

using MS abundance ratio m/z 170:175 as a discriminator: m/z 170 indicates creatine K^+ and m/z 175 indicates protonated arginine. The ROC cutoff was optimized at 2.56, with a sensitivity, specificity, and accuracy of 92, 81, and 86%, respectively. Wilcoxon rank-sum test indicated a statistically significant result (p value < 0.001). **e** Box plot using the fragment ion ratio m/z 87:60 as a discriminator, comparing the GABA-associated transition to that of choline. The ROC cutoff was optimized at 0.26, with a sensitivity, specificity, and accuracy of 92, 88, and 90%, respectively. Wilcoxon rank-sum test indicated a statistically significant result (p value < 0.001)

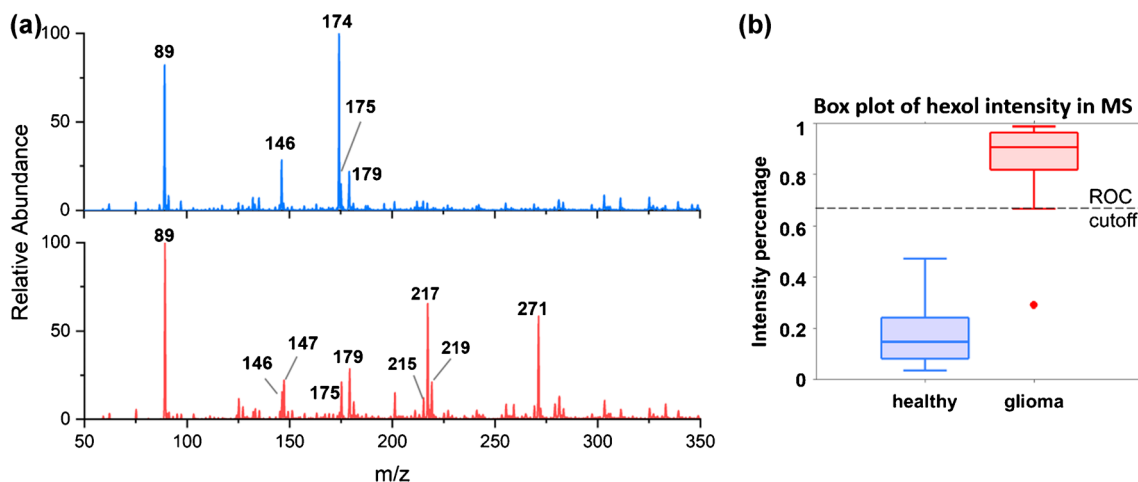


Fig. 5 **a** Negative-mode DESI-MS mass spectra for a representative healthy (blue) and glioma (red) tissue smear. **b** Box plot using the intensity percentage of hexol (as defined in Eq. 1) as a discriminator. The ROC

cutoff was optimized at 0.67, with a sensitivity, specificity, and accuracy of 92, 100, and 97%, respectively. Wilcoxon rank-sum test indicated a statistically significant result (p value < 0.001)

molecule ($[M - H]^-$, m/z 181). To better characterize the abundance ratio between all hexol-related species and NAA, the intensity percentage of hexol is used. (1)

$$\begin{aligned} \% \text{Intensity}_{\text{hexol}} &= \frac{I_{\text{total hexol}}}{I_{\text{NAA}} + I_{\text{total hexol}}} \quad (1) \\ &= \frac{I_{181} + I_{217} + I_{219} + I_{271}}{(I_{174}) + (I_{181} + I_{217} + I_{219} + I_{271})} * 100\% \end{aligned}$$

Figure 5b shows the box plot of this intensity percentage with good separation between the two tissue types. Similarly, the optimal cutoff was determined based on ROC, yielding a sensitivity, specificity, and accuracy of 92, 100, and 97%, respectively. Wilcoxon rank-sum test showed that hexol-related species were significantly upregulated in glioma samples (p value < 0.001). NAA intensities were also calculated to allow comparison with the performance of the current intraoperative DESI method. Illustrated in Supplementary information Fig. S5, NAA alone is powerful enough to distinguish glioma from normal tissue with sensitivity, specificity, and accuracy values of 100, 88, and 93%. The improved diagnostic accuracy obtained by characterizing hexol intensity percentage (96%), compared to NAA measurement (93%), suggests that the inclusion of an inversely related metabolite can increase diagnostic power over that for a single biomarker. While the three diagnostic ratios in the positive-ion mode have comparable accuracies to the existing NAA measurement (93, 86, 90%, respectively), their inclusion in the new method offers multiple diagnosis channels to ensure a robust prediction. This expectation remains to be tested on a large number of samples and in an intraoperative setting where a wider range of tissue types is likely to be encountered.

Conclusions

The inclusion of additional biomarkers in a DESI-MS method will likely improve the diagnostic accuracy and method robustness of distinguishing brain parenchyma from glioma. In this study, metabolic biomarkers of healthy brain tissue and glioma have been discovered by both full-scan MS profiling and MRM profiling using nESI. The most diagnostic and abundant are GABA, creatine, glutamic acid, carnitine, and hexol. Good separation between the two tissue types has been observed in PCA score plots and box plots. With the goal of using these metabolites for rapid tissue diagnosis, new DESI-MS methods (taking 5 min) have been developed and tested using brain smears. Several diagnostic ion abundance ratios, generated both from intact ions in full-scan mass spectra and from fragment ions in MS/MS spectra, have been identified. The positive-mode abundance ratios (full-scan MS and MS/MS) related to GABA, carnitine, and creatine all display >

90% sensitivities, > 80% specificities, and > 85% accuracies for tissue diagnosis at their optimized ROC cutoffs. Further, the negative-mode abundance ratio of hexol shows good discrimination, with a sensitivity, specificity, and accuracy of 92, 100, and 97%, respectively. We envision that integrating these discriminatory metabolites into the current intraoperative DESI-MS methodology will provide a more sensitive detection of glioma near infiltrative margins and ultimately assist the achievement of gross total tumor resection during surgeries.

Supplementary Information The online version contains supplementary material available at <https://doi.org/10.1007/s00216-021-03593-0>.

Acknowledgements The authors thank Dr. Eyas M. Hattab for providing evaluation of brain samples used in this and previous work. We thank Clint M. Alfaro for his assistance in writing custom MATLAB codes for data processing and Christina R. Ferreira for providing the scan library used in multiple reaction monitoring (MRM) profiling.

Code availability The custom MATLAB codes used for data processing are available from the corresponding author upon request.

Author contribution R. Chen and R.G. Cooks designed the research; R. Chen performed the research; R. Chen and H.M. Brown analyzed the data; R. Chen, H.M. Brown, and R.G. Cooks wrote the paper.

Funding This work was funded by National Cancer Institute (IR33CA240181-01A1) and Waters Inc. (Grant #40002775).

Data availability All data analyzed during this study are included in this published article and its electronic supplementary information.

Declarations

Ethics approval Not applicable.

Consent to participate Not applicable.

Consent for publication Not applicable.

Conflict of interest The authors declare no competing interests.

References

1. Minniti G, Muni R, Lanzetta G, Marchetti P, Enrici RM. Chemotherapy for glioblastoma: current treatment and future perspectives for cytotoxic and targeted agents. *Anticancer Res.* 2009;29(12):5171–84.
2. Chaichana KL, Cabrera-Aldana EE, Jusue-Torres I, Wijesekera O, Olivi A, Rahman M, et al. When gross total resection of a glioblastoma is possible, how much resection should be achieved? *World Neurosurg.* 2014;82(1-2):e257–65 Available from. <https://doi.org/10.1016/j.wneu.2014.01.019>.
3. Jermyn M, Mok K, Mercier J, Desroches J, Pichette J, Saint-Arnaud K, et al. Intraoperative brain cancer detection with Raman spectroscopy in humans. *Sci Transl Med.* 2015;7(274):274ra19 Available from. <https://doi.org/10.1126/scitranslmed.aaa2384>.

4. Reinges MH, Nguyen HH, Krings T, Hutter BO, Rohde V, Gilsbach JM. Course of brain shift during microsurgical resection of supratentorial cerebral lesions: limits of conventional neuronavigation. *Acta Neurochir.* 2004;146(4):369–77; discussion 77. Available from: <https://doi.org/10.1007/s00701-003-0204-1>.
5. Ogrinc N, Saudemont P, Takats Z, Salzert M, Fournier I. Cancer surgery 2.0: guidance by real-time molecular technologies. *Trends Mol Med.* 2021;27(6):602–15. Available from: <https://doi.org/10.1016/j.molmed.2021.04.001>.
6. Brat DJ, Verhaak RG, Aldape KD, Yung WK, Salama SR, Cooper LA, et al. Comprehensive, integrative genomic analysis of diffuse lower-grade gliomas. *N Engl J Med.* 2015;372(26):2481–98. Available from: <https://doi.org/10.1056/NEJMoa1402121>.
7. Stummer W, Koch R, Valle RD, Roberts DW, Sanai N, Kalkanis S, et al. Intraoperative fluorescence diagnosis in the brain: a systematic review and suggestions for future standards on reporting diagnostic accuracy and clinical utility. *Acta Neurochir.* 2019;161(10):2083–98. Available from: <https://doi.org/10.1007/s00701-019-04007-y>.
8. Stummer W, Pichlmeier U, Meinel T, Wiestler OD, Zanella F, Reulen H-J. Fluorescence-guided surgery with 5-aminolevulinic acid for resection of malignant glioma: a randomised controlled multicentre phase III trial. *The Lancet Oncology.* 2006;7(5):392–401. Available from: [https://doi.org/10.1016/s1470-2045\(06\)70665-9](https://doi.org/10.1016/s1470-2045(06)70665-9).
9. Valdes PA, Juvekar P, Agar NYR, Gioux S, Golby AJ. Quantitative wide-field imaging techniques for fluorescence guided neurosurgery. *Front Surg.* 2019;6:31. Available from: <https://doi.org/10.3389/fsurg.2019.00031>.
10. Hollon T, Lewis S, Freudiger CW, Sunney Xie X, Orringer DA. Improving the accuracy of brain tumor surgery via Raman-based technology. *Neurosurg Focus.* 2016;40(3):E9. Available from: <https://doi.org/10.3171/2015.12.FOCUS15557>.
11. Hollon TC, Pandian B, Adapa AR, Urias E, Save AV, Khalsa SSS, et al. Near real-time intraoperative brain tumor diagnosis using stimulated Raman histology and deep neural networks. *Nat Med.* 2020;26(1):52–8. Available from: <https://doi.org/10.1038/s41591-019-0715-9>.
12. Hänel L, Kwiatkowski M, Heikaus L, Schluter H. Mass spectrometry-based intraoperative tumor diagnostics. *Future Sci OA.* 2019;5(3):FSO373. Available from: <https://doi.org/10.4155/fsoa-2018-0087>.
13. Zhang J, Rector J, Lin JQ, Young JH, Sans M, et al. Nondestructive tissue analysis for ex vivo and in vivo cancer diagnosis using a handheld mass spectrometry system. *Sci Transl Med.* 2017;9(406). Available from: <https://doi.org/10.1126/scitranslmed.aan3968>.
14. Sans M, Zhang J, Lin JQ, Feider CL, Giese N, Breen MT, et al. Performance of the MasSpec pen for rapid diagnosis of ovarian cancer. *Clin Chem.* 2019;65(5):674–83. Available from: <https://doi.org/10.1373/clinchem.2018.299289>.
15. Woolman M, Kuzan-Fischer CM, Ferry I, Kiyota T, Luu B, Wu M, et al. Picosecond infrared laser desorption mass spectrometry identifies medulloblastoma subgroups on intrasurgical timescales. *Cancer Res.* 2019;79(9):2426–34. Available from: <https://doi.org/10.1158/0008-5472.CAN-18-3411>.
16. Woolman M, Qiu J, Kuzan-Fischer CM, Ferry I, Dara D, Katz L, et al. In situ tissue pathology from spatially encoded mass spectrometry classifiers visualized in real time through augmented reality. *Chem Sci.* 2020;11(33):8723–35. Available from: <https://doi.org/10.1039/d0sc02241a>.
17. Ogrinc N, Saudemont P, Balog J, Robin YM, Gimeno JP, Pascal Q, et al. Water-assisted laser desorption/ionization mass spectrometry for minimally invasive in vivo and real-time surface analysis using SpiderMass. *Nat Protoc.* 2019;14(11):3162–82. Available from: <https://doi.org/10.1038/s41596-019-0217-8>.
18. Vaysse PM, Kooreman LFS, Engelen SME, Kremer B, Olde Damink SWM, Heeren RMA, et al. Stromal vapors for real-time molecular guidance of breast-conserving surgery. *Sci Rep.* 2020;10(1):20109. Available from: <https://doi.org/10.1038/s41598-020-77102-1>.
19. Takáts Z, Wiseman JM, Gologan B, Cooks RG. Mass spectrometry sampling under ambient conditions with desorption electrospray ionization. *Science.* 2004;306(5695):471–3. Available from: <https://doi.org/10.1126/science.1104404>.
20. Jarmusch AK, Alfaro CM, Pirro V, Hattab EM, Cohen-Gadol AA, Cooks RG. Differential lipid profiles of normal human brain matter and gliomas by positive and negative mode desorption electrospray ionization - mass spectrometry imaging. *PLoS One.* 2016;11(9):e0163180. Available from: <https://doi.org/10.1371/journal.pone.0163180>.
21. Akbari Lakeh M, Tu A, Muddiman DC, Abdollahi H. Discriminating normal regions within cancerous hen ovarian tissue using multivariate hyperspectral image analysis. *Rapid Commun Mass Spectrom.* 2019;33(4):381–91. Available from: <https://doi.org/10.1002/rcm.8362>.
22. Eberlin LS, Dill AL, Golby AJ, Ligon KL, Wiseman JM, Cooks RG, et al. Discrimination of human astrocytoma subtypes by lipid analysis using desorption electrospray ionization mass spectrometry. *Angew Chem Int Ed Eng.* 2010;49(34):5953–6. Available from: <https://doi.org/10.1002/anie.201001452>.
23. Eberlin LS, Margulis K, Planell-Mendez I, Zare RN, Tibshirani R, Longacre TA, et al. Pancreatic cancer surgical resection margins: molecular assessment by mass spectrometry imaging. *PLoS Med.* 2016;13(8):e1002108. Available from: <https://doi.org/10.1371/journal.pmed.1002108>.
24. Santoro AL, Drummond RD, Silva IT, Ferreira SS, Juliano L, Vendramini PH, et al. In situ DESI-MSI lipidomic profiles of breast cancer molecular subtypes and precursor lesions. *Cancer Res.* 2020;80(6):1246–57. Available from: <https://doi.org/10.1158/0008-5472.CAN-18-3574>.
25. Jarmusch AK, Pirro V, Baird Z, Hattab EM, Cohen-Gadol AA, Cooks RG. Lipid and metabolite profiles of human brain tumors by desorption electrospray ionization-MS. *Proc Natl Acad Sci U S A.* 2016;113(6):1486–91. Available from: <https://doi.org/10.1073/pnas.1523306113>.
26. Pirro V, Alfaro CM, Jarmusch AK, Hattab EM, Cohen-Gadol AA, Cooks RG. Intraoperative assessment of tumor margins during glioma resection by desorption electrospray ionization-mass spectrometry. *Proc Natl Acad Sci U S A.* 2017;114(26):6700–5. Available from: <https://doi.org/10.1073/pnas.1706459114>.
27. Brown HM, Alfaro CM, Pirro V, Dey M, Hattab EM, Cohen-Gadol AA, et al. Intraoperative mass spectrometry platform for IDH mutation status prediction, glioma diagnosis, and estimation of tumor cell infiltration. *J Appl Lab Med.* 2021;6(4):902–16. Available from: <https://doi.org/10.1093/jalm/jfaa233>.
28. Cordeiro FB, Jarmusch AK, Leon M, Ferreira CR, Pirro V, Eberlin LS, et al. Mammalian ovarian lipid distributions by desorption electrospray ionization-mass spectrometry (DESI-MS) imaging. *Anal Bioanal Chem.* 2020;412(6):1251–62. Available from: <https://doi.org/10.1007/s00216-019-02352-6>.
29. Eberlin LS, Tibshirani RJ, Zhang J, Longacre TA, Berry GJ, Bingham DB, et al. Molecular assessment of surgical-resection margins of gastric cancer by mass-spectrometric imaging. *Proc Natl Acad Sci U S A.* 2014;111(7):2436–41. Available from: <https://doi.org/10.1073/pnas.1400274111>.
30. Eberlin LS, Ferreira CR, Dill AL, Ifá DR, Cooks RG. Desorption electrospray ionization mass spectrometry for lipid characterization and biological tissue imaging. *Biochim Biophys Acta.* 2011;1811(11):946–60. Available from: <https://doi.org/10.1016/j.bbali.2011.05.006>.

31. Pirro V, Jarmusch AK, Alfaro CM, Hattab EM, Cohen-Gadol AA, Cooks RG. Utility of neurological smears for intrasurgical brain cancer diagnostics and tumour cell percentage by DESI-MS. *Analyst*. 2017;142(3):449–54. Available from: <https://doi.org/10.1039/c6an02645a>.
32. Tousignant KD, Rockstroh A, Poad BLJ, Talebi A, Young RSE, Taherian Fard A, et al. Therapy-induced lipid uptake and remodeling underpin ferroptosis hypersensitivity in prostate cancer. *Cancer Metab*. 2020;8:11. Available from: <https://doi.org/10.1186/s40170-020-00217-6>.
33. Young RSE, Bowman AP, Williams ED, Tousignant KD, Bidgood CL, Narreddula VR, et al. Apocryphal FADS2 activity promotes fatty acid diversification in cancer. *h*. 2021;34(6):108738. Available from: <https://doi.org/10.1016/j.celrep.2021.108738>.
34. Andersen MK, Høiem TS, Claes BSR, Balluff B, Martin-Lorenzo M, Richardsen E, et al. Spatial differentiation of metabolism in prostate cancer tissue by MALDI-TOF MSI. *Cancer Metab*. 2021;9(1):9. Available from: <https://doi.org/10.1186/s40170-021-00242-z>.
35. Bi J, Chowdhry S, Wu S, Zhang W, Masui K, Mischel PS. Altered cellular metabolism in gliomas - an emerging landscape of actionable co-dependency targets. *Nat Rev Cancer*. 2020;20(1):57–70. Available from: <https://doi.org/10.1038/s41568-019-0226-5>.
36. Pandey R, Caflisch L, Lodi A, Brenner AJ, Tiziani S. Metabolomic signature of brain cancer. *Mol Carcinog*. 2017;56(11):2355–71. Available from: <https://doi.org/10.1002/mc.22694>.
37. Alfaro CM, Pirro V, Keating MF, Hattab EM, Cooks RG, Cohen-Gadol AA. Intraoperative assessment of isocitrate dehydrogenase mutation status in human gliomas using desorption electrospray ionization-mass spectrometry. *J Neurosurg*. 2019:1–8. Available from: <https://doi.org/10.3171/2018.8.JNS181207>.
38. Nakamizo S, Sasayama T, Shinohara M, Irino Y, Nishiumi S, Nishihara M, et al. GC/MS-based metabolomic analysis of cerebrospinal fluid (CSF) from glioma patients. *J Neuro-Oncol*. 2013;113(1):65–74. Available from: <https://doi.org/10.1007/s11060-013-1090-x>.
39. Kampa JM, Kellner U, Marsching C, Ramallo Guevara C, Knappe UJ, Sahin M, et al. Glioblastoma multiforme: metabolic differences to peritumoral tissue and IDH-mutated gliomas revealed by mass spectrometry imaging. *Neuropathology*. 2020;40(6):546–58. Available from: <https://doi.org/10.1111/neup.12671>.
40. Yan X, Zhao X, Zhou Z, McKay A, Brunet A, Zare RN. Cell-type-specific metabolic profiling achieved by combining desorption electrospray ionization mass spectrometry imaging and immunofluorescence staining. *Anal Chem*. 2020;92(19):13281–9. Available from: <https://doi.org/10.1021/acs.analchem.0c02519>.
41. Banerjee S, Zare RN, Tibshirani RJ, Kunder CA, Nolley R, Fan R, et al. Diagnosis of prostate cancer by desorption electrospray ionization mass spectrometric imaging of small metabolites and lipids. *Proc Natl Acad Sci U S A*. 2017;114(13):3334–9. Available from: <https://doi.org/10.1073/pnas.1700677114>.
42. Bulik M, Jancalek R, Vanicek J, Skoch A, Mechl M. Potential of MR spectroscopy for assessment of glioma grading. *Clin Neurol Neurosurg*. 2013;115(2):146–53. Available from: <https://doi.org/10.1016/j.clineuro.2012.11.002>.
43. Long PM, Moffett JR, Nambodiri AMA, Viapiano MS, Lawler SE, Jaworski DM. N-acetylaspartate (NAA) and N-acetylaspartylglutamate (NAAG) promote growth and inhibit differentiation of glioma stem-like cells. *J Biol Chem*. 2013;288(36):26188–200. Available from: <https://doi.org/10.1074/jbc.M113.487553>.
44. Moffett JR, Arun P, Ariyannur PS, Nambodiri AM. N-Acetylaspartate reductions in brain injury: impact on post-injury neuroenergetics, lipid synthesis, and protein acetylation. *Front Neuroenerg*. 2013;5:11. Available from: <https://doi.org/10.3389/fnene.2013.00011>.
45. Robert SM, Sontheimer H. Glutamate transporters in the biology of malignant gliomas. *Cell Mol Life Sci*. 2014;71(10):1839–54. Available from: <https://doi.org/10.1007/s00018-013-1521-z>.
46. Rackayova V, Cudalbu C, Pouwels PJW, Braissant O. Creatine in the central nervous system: from magnetic resonance spectroscopy to creatine deficiencies. *Anal Biochem*. 2017;529:144–57. Available from: <https://doi.org/10.1016/j.ab.2016.11.007>.
47. Jothi J, Janardhanam VA, Krishnaswamy R. Metabolic variations between low-grade and high-grade gliomas-profiling by (1)H NMR spectroscopy. *J Proteome Res*. 2020;19(6):2483–2490. Available from: <https://doi.org/10.1021/acs.jproteome.0c00243>.
48. Cai K, Tain RW, Zhou XJ, Damen FC, Scotti AM, Hariharan H, et al. Creatine CEST MRI for differentiating gliomas with different degrees of aggressiveness. *Mol Imaging Biol*. 2017;19(2):225–32. Available from: <https://doi.org/10.1007/s11307-016-0995-0>.
49. Shao W, Gu J, Huang C, Liu D, Huang H, Huang Z, et al. Malignancy-associated metabolic profiling of human glioma cell lines using 1H NMR spectroscopy. *Mol Cancer*. 2014;13:197. Available from: <https://doi.org/10.1186/1476-4598-13-197>.
50. Song X, Yang X, Narayanan R, Shankar V, Ethiraj S, Wang X, et al. Oral squamous cell carcinoma diagnosed from saliva metabolic profiling. *Proc Natl Acad Sci U S A*. 2020;117(28):16167–73. Available from: <https://doi.org/10.1073/pnas.2001395117>.
51. Wittmann BM, Stirdivant SM, Mitchell MW, Wulff JE, McDunn JE, Li Z, et al. Bladder cancer biomarker discovery using global metabolomic profiling of urine. *PLoS One*. 2014;9(12):e115870. Available from: <https://doi.org/10.1371/journal.pone.0115870>.
52. Patra S, Ghosh A, Roy SS, Bera S, Das M, Talukdar D, et al. A short review on creatine-creatine kinase system in relation to cancer and some experimental results on creatine as adjuvant in cancer therapy. *Amino Acids*. 2012;42(6):2319–30. Available from: <https://doi.org/10.1007/s00726-011-0974-3>.
53. Jung E, Alfonso J, Osswald M, Monyer H, Wick W, Winkler F. Emerging intersections between neuroscience and glioma biology. *Nat Neurosci*. 2019;22(12):1951–60. Available from: <https://doi.org/10.1038/s41593-019-0540-y>.
54. Fink MA, Paland H, Herzog S, Grube M, Vogelgesang S, Weitmann K, et al. L-carnitine-mediated tumor cell protection and poor patient survival associated with OCTN2 overexpression in glioblastoma multiforme. *Clin Cancer Res*. 2019;25(9):2874–86. Available from: <https://doi.org/10.1158/1078-0432.CCR-18-2380>.
55. Melone MAB, Valentino A, Margarucci S, Galderisi U, Giordano A, Peluso G. The carnitine system and cancer metabolic plasticity. *Cell Death Dis*. 2018;9(2):228. Available from: <https://doi.org/10.1038/s41419-018-0313-7>.
56. Harder BG, Blomquist MR, Wang J, Kim AJ, Woodworth GF, Winkles JA, et al. Developments in blood-brain barrier penetrance and drug repurposing for improved treatment of glioblastoma. *Front Oncol*. 2018;8:462. Available from: <https://doi.org/10.3389/fonc.2018.00462>.
57. Xie Z, Ferreira CR, Virequ AA, Cooks RG. Multiple reaction monitoring profiling (MRM profiling): small molecule exploratory analysis guided by chemical functionality. *Chem Phys Lipids*. 2021;235:105048. Available from: <https://doi.org/10.1016/j.chemphyslip.2021.105048>.
58. Sündermann A, Eggers LF, Schwudke D. Liquid extraction: Blich and Dyer. In: Wenk MR, editor. *Encyclopedia of lipidomics*. Dordrecht: Springer Netherlands; 2016. p. 1–4.
59. Brown HM, Pu F, Dey M, Miller J, Shah MV, Shapiro SA, et al. Intraoperative detection of isocitrate dehydrogenase mutations in human gliomas using a miniature mass spectrometer. *Anal Bioanal Chem*. 2019. Available from: <https://doi.org/10.1007/s00216-019-02198-y>.

60. Manicke NE, Kistler T, Ifa DR, Cooks RG, Ouyang Z. High-throughput quantitative analysis by desorption electrospray ionization mass spectrometry. *J Am Soc Mass Spectrom.* 2009;20(2): 321–5. Available from: <https://doi.org/10.1016/j.jasms.2008.10.011>.

Publisher's note Springer Nature remains neutral with regard to jurisdictional claims in published maps and institutional affiliations.



Rong Chen is a Ph.D. candidate in analytical chemistry under the supervision of Prof. Graham Cooks of Purdue University. Her research interest lies in the discovery and measurement of molecular biomarkers for rapid tissue diagnosis by mass spectrometry.



Hannah Marie Brown is a graduate researcher in Dr. R. Graham Cooks' laboratory in the Department of Chemistry of Purdue University. Her research focuses on developments of ambient ionization mass spectrometry for intraoperative and high-throughput brain cancer diagnostics.



R. Graham Cooks is Henry Bohn Hass Distinguished Professor of Chemistry of Purdue University. His career has been devoted to realizing new concepts in mass spectrometry through instrumentation and their real-world applications. After early work in desorption ionization and tandem mass spectrometry, he has focused on accelerated reactions in droplets, high-throughput analysis, and synthesis using molecular ions. The use of desorption electrospray ionization (DESI) in cancer diagnosis is a current interest.